# Static and dynamic angles of repose in loose granular materials under reduced gravity

M. G. Kleinhans,[1] H. Markies,[1] S. J. de Vet,[2] A. C. in 't Veld,[3] and F. N. Postema[3]

Received 30 May 2011; revised 6 September 2011; accepted 15 September 2011; published 17 November 2011.

[1] Granular materials avalanche when a static angle of repose is exceeded and freeze at a dynamic angle of repose. Such avalanches occur subaerially on steep hillslopes and wind dunes and subaqueously at the lee side of deltas. Until now it has been assumed that the angles of repose are independent of gravitational acceleration. The objective of this work is to experimentally determine whether the angles of repose depend on gravity. In 33 parabolic flights in a well-controlled research aircraft we recorded avalanching granular materials in rotating drums at effective gravitational accelerations of 0.1, 0.38 and 1.0 times the terrestrial value. The granular materials varied in particle size and rounding and had air or water as interstitial fluid. Materials with angular grains had time-averaged angles of about 40° and with rounded grains about 25° for all effective gravitational accelerations, except the finest glass beads in air, which was explained by static electricity. For all materials, the static angle of repose *in*creases about 5° with reduced gravity, whereas the dynamic angle *de*creases with about 10°. Consequently, the avalanche size increases with reduced gravity. The experimental results suggest that relatively low slopes of granular material on Mars may have formed by dry flows without a lubricating fluid. On asteroids even lower slopes are expected. The dependence on gravity of angle of repose may require reanalysis of models for many phenomena involving sediment, also at much lower slope angles.

**Citation:** Kleinhans, M. G., H. Markies, S. J. de Vet, A. C. in 't Veld, and F. N. Postema (2011), Static and dynamic angles of repose in loose granular materials under reduced gravity, *J. Geophys. Res.*, *116*, E11004, doi:10.1029/2011JE003865.

## 1. Introduction

### 1.1. Problem Definition and Objective

[2] A basic property of noncohesive granular materials is the angle of repose: the maximum slope angle at which the material is at rest [*Lowe*, 1976]. Above this slope angle, the material starts to flow; below this angle, the material is stable. The angle varies from 25° for smooth spherical particles to 45° for rough angular particles [*Carrigy*, 1970; *Pohlman et al.*, 2006]. Noncohesive granular materials are found in many contexts, from kitchen to industry and nature (Figure 1). Geomorphologically relevant examples are scree and talus slopes, but even these are, on Earth at least, affected by interstitial fluid or ice. Dry flows may have occurred on Earth, Mars, moons and asteroids [*Chuang and Greeley*, 2000; *Bart*, 2007; *Dundas et al.*, 2010], on wind-blown dunes. Entirely submerged flows for which nearly the same angle of repose is observed are found on the lee slope of subaqueous dunes and the subaqueous slopes of deltas [e.g., *Kleinhans*, 2004, 2010].

[3] The angle of repose is an empirical friction parameter that is essential in models of numerous phenomena involving granular material, most of them actually at slopes much lower than the angle of repose. The angle of repose is therefore relevant for many geomorphological phenomena which is illustrated with the following examples.

[4] 1. Subaerial granular avalanche features on Mars have angles that potentially contain information on material properties through the rheological properties [*Gerstell et al.*, 2004; *Pirulli and Mangeney*, 2008], including the presence of water. Relatively low fan angles formed from gullies have been interpreted to be the lubricating effect of water [*Harrison and Grimm*, 2003; *Heldmann and Mellon*, 2004; *Dickson et al.*, 2007; *Kreslavsky and Head*, 2009]. Mud flows on Mars and Venus may also have larger runout lengths than on Earth [*Rickenmann*, 1999; *Malin*, 1992], which remains poorly explained [*Lucas and Mangeney*, 2007].

[5] 2. The subaqueous angles of static and dynamic repose are similar to the subaerial values, and the difference between static and dynamic angles leads to discrete avalanches at the lee side of dunes, bars and deltas in fluvial and coastal environments [*Kleinhans*, 2004]. This avalanching, in turn, causes a basic particle size-sorting pattern depending on the angles of repose of the particle mixture [*Boutreux et al.*, 1998; *Makse et al.*, 1998]. Such sorting patterns are ubiquitous in deposits and outcrops and greatly affect the morphodynamics in rivers and deltas [e.g., *Kleinhans*, 2004, 2005a].

[1]Faculty of Geosciences, Utrecht University, Utrecht, Netherlands.
[2]Institute for Biodiversity and Ecosystem Dynamics, University of Amsterdam, Amsterdam, Netherlands.
[3]Faculty of Aerospace Engineering, Delft University of Technology, Delft, Netherlands.


0148-0227/11/2011JE003865

**Figure 1.** A pile of rounded gravel at the angle of repose, built by Gijsbert F. Kleinhans.

[6] 3. The downstream angle of subaqueous delta slopes on Mars is an important indicator of the magnitude and duration of the flow that created it. Steep angles indicate low ('bed-load') sediment transport rates and long duration, whereas gentler slopes indicate higher ('suspended') transport rates and shorter formative time periods [*Jopling*, 1964; *Allen*, 1970]. Such interpretation has relevance for use of deltas as indicators of paleo-hydrological conditions [*Kleinhans*, 2010; *Kleinhans et al.*, 2010].

[7] 4. Fluvial and coastal models for beginning of sediment motion, sediment fluidization and sediment transport on horizontal beds and gentle slopes include the angle of repose as a Coulomb friction angle [*Bagnold*, 1951; *Allen and Leeder*, 1980; *Parker and Andrews*, 1985; *Wiberg and Smith*, 1987; *Soulsby and Damgaard*, 2005; *Vollmer and Kleinhans*, 2007].

[8] 5. Impact crater collapse depends on the angle of repose of the material [*Melosh and Ivanov*, 1999].

[9] Until now it has been assumed in planetary morphology and geology that the angle of repose of a non-cohesive granular material is independent of gravity, i.e. has the same angle on other planets as on Earth. Given the importance of this angle it is surprising that the hypothesis of independence of gravity has hardly been tested. The few experiments recorded in literature that did test it have contradicting results varying from opposite effects to no effect at all. However, the lack of data is understandable as the practical difficulties of doing controlled experiments in reduced gravity are significant. As a first attempt to address the question whether the angle of repose is really independent of gravity, we designed experiments for the straightforward case of dense granular flows in discrete avalanches.

[10] The objective of this paper is to experimentally determine whether the static and dynamic angles of repose depend on gravity, in order to gain understanding of granular avalanches under gravity lower than on Earth. We will measure the angle of repose systematically for well-rounded and for angular particles, for small and large particles, for particles in air and in water, and for three different relative gravitational accelerations, henceforth g-levels: $g = 1$ (Earth), $g = 0.38$ (Mars) and $g = 0.1$ (practical lower limit), where $g = g_{eff}/g_e$ with $g_{eff}$ = effective gravitational acceleration and $g_e$ = gravitational acceleration on Earth (9.81 m/s$^2$).

[11] We first discuss the contradicting data reported in literature, then elaborate on possible causes and working hypotheses. After that, we present our methods and results. These are followed by discussion and relevance of results compared to literature, and conclusions.

### 1.2. Previous Experiments

[12] Angles of repose were determined in three different manners in the past. First, experiments were done with various granular materials to determine the angle of repose as a function of material properties [*Carrigy*, 1970; *Dury et al.*, 1998; *Brucks et al.*, 2007], and to determine direct relations between the angle of repose, runout length and dynamics [e.g., *Rickenmann*, 1999; *Mangeney et al.*, 2010]. This has hardly been done for reduced gravity, partly because analyses and modeling studies demonstrated or assumed that it is independent of gravity [e.g., *Zhou et al.*, 2001; *Mangeney-Castelnau et al.*, 2005]. Second, slope angles of dry or submerged dense granular flow deposits were measured in nature, including on other planets and the Moon [e.g., *Malin*, 1992; *Kreslavsky and Head*, 2009]. Third, physics-based numerical models were run whereby resulting morphology and dynamics such as velocity and runout length were matched to a real case by calibrating the angle of repose [e.g., *Harrison and Grimm*, 2003; *Pirulli and Mangeney*, 2008]. The second and third approach were done for reduced gravity, but, working from natural examples, suffer from under-determination of the possible causes for different angles due to gravity. Particularly the unknown presence of pore water as lubrication could lead to much lower angles than expected from dry granular flows. Similarly, runout lengths of large landslides on Mars were longer than expected and another hitherto unidentified factor could be involved [*Lucas and Mangeney*, 2007], potentially the angle of repose.

[13] Recent centrifuge experiments with rotating drums suggest a negligible effect of gravity on angle of repose [*Brucks et al.*, 2007]. These were done with glass beads with $D = 0.53$ mm, where $D$ = particle diameter with $1 < g < 25$. A rotating drum partially filled with granular material can represent various avalanching phenomena. In slow rotation, the angle of the material will increase until the static angle of repose is exceeded, and will avalanche until it freezes from the downstream end upwards at the dynamic angle of repose [*Carrigy*, 1970; *Dury et al.*, 1998; *Brucks et al.*, 2007]. This mode is called discrete avalanching regime. For increasing rotation rate, the avalanching becomes continuous at the dynamic angle of repose, sometimes called rolling flow regime, and the slope starts to deviate from a straight line. At very high rotation rates the slope develops and S-shape with inertial overshoot of particles at the top of the pile, which is called cascading regime. For high enough rotation rates the material is centrifuged to the periphery of the drum and avalanching ceases. In the well-controlled centrifuge experiments of *Brucks et al.* [2007] the transition from the avalanching to the rolling state was found to be largely independent on the effective gravity for glass beads. The thickness of the continuous flowing layer was also nearly independent of gravitational level, while the flow velocity scaled with $\sqrt{g_{eff}}$. The angle of repose was found to depend nonlinearly on a Froude number $Fr = \omega^2 R/g_{eff}$,

where $\omega$ = angular frequency of the cylinder and $R$ = radius of the drum. For $10^{-6} < Fr < 10^{-3}$ the angle of repose did not vary more than a few degrees, while this range covers the discrete avalanche regime to the cascading regime. For larger $Fr$ the angle of repose increased rapidly [*Brucks et al.*, 2007].

[14] In contrast, the relatively poorly controlled experiments in parabolic flights by *Klein and White* [1990] showed that the dynamic angle of repose decreases linearly with increasing $\sqrt{g}$ for both glass beads of $D$ = 1.35 mm and beach sand of $D$ = 0.4 mm, although nearly a factor of twice less for the latter. The data indicate that the effect of gravity is larger for $g < 1$ but barely noticeable for $g > 1$, which could explain why the effect is not obvious in centrifuges. These data were collected with rotating drums at nearly constant $\omega$ in parabolic flights with $0.1 < g < 1.9$ (see *Walton et al.* [2007] for reanalysis and discussion). *Klein and White* [1990] hypothesized that in reduced gravity, inter-particle normal loads decreased which increased particle friction coefficients, so that the angle of repose increased. However, *Walton et al.* [2007] suggested that some contact force may have increased, particularly as the glass beads with larger contact surface areas showed a stronger trend. 'Contact force' can be composed of many components; here static electricity or capillary force by microscopic pockets of water could be significant.

[15] In short, a data set at decreased gravity collected in parabolic flights shows a strong trend of increasing angle of repose for decreasing gravity [*Klein and White*, 1990] whereas data sets for increased gravity collected in a centrifuge shows no effect [*Brucks et al.*, 2007]. For decreasing gravity the relative importance of contact forces could not be excluded. This point is important, because the aim of the experiments in this paper is to assess the effect of reduced gravity on the angle of repose, and to be representative for natural systems with similar to much larger particles, both subaerial and subaqueous. It will be essential to perform the experiments both subaerially and subaqueously because the latter condition excludes significant electrostatic effects and capillary effects, although it adds drag effects.

### 1.3. Hypothesis Development

[16] The general belief that the angle of repose is independent of gravity is perhaps derived from two classical laws: the Coulomb law and the first law of Amontons. The Coulomb law states that kinetic friction is independent of the sliding velocity. This implies that the angle of repose is the same for granular matter in motion and in rest. Simplistically, we might assume that this is the angle a particle must pivot over underlying particles to move down-slope. The first law of Amontons states that the force of friction is directly proportional to the applied load. A hypothetical pile of spheres is stable despite the increasing load with depth into the pile, because the friction increases with the load. This implies that a reduction of applied load under lower gravity leads to equally lower friction, so that the static angle of repose remains constant. Furthermore, by combination with the Coulomb law it follows that a granular flow the driving gravitational force along the slope, $F_z = mg_{eff} \sin\alpha$, is balanced by friction, which depends on the force normal to the slope, $F_f = mg_{eff} \cos\alpha$, where $\alpha$ = angle of repose. As both scale with the weight of the flow, the dynamic angle of repose for a granular flow is again independent of gravity.

[17] However, this oversimplifies the processes. Since Coulomb it has been found that static friction is larger than dynamic friction. For the initiation of a granular flow, the static angle of repose must be exceeded that is larger than the dynamic angle of repose. So the friction effectively depends on flow depth and velocity [e.g., *Pouliquen*, 1999; *Jop et al.*, 2006], particle roughness [*Pohlman et al.*, 2006], and sorting (also called polydispersity) (see *Kleinhans* [2004] for review) [*Kleinhans*, 2005a; *Goujon et al.*, 2007].

[18] The static angle of repose may be related to cohesive forces including Vanderwaals forces, electrostatic forces and capillary forces in case of microscopic fluid pockets between the particles. We will not attempt to unravel the combined forces but aim at excluding those which are due to experimental effects but unlikely to be important in granular materials in nature. We may assume that these forces also act for vanishing gravity and that the arrested granular material attains a packing density independently of gravity as suggested by *Brucks et al.* [2007]. We therefore hypothesize that the static angle of repose increases with decreasing gravity.

[19] The dynamic angle of repose is the product of a granular flow. Mobilization of the material into a moving avalanche necessarily involves dilatation, which reduces the number of contacts and therefore the contact forces. Once a granular flow is moving, the momentum and reduced friction cause it to run out below the static angle of repose to freeze at the dynamic angle of repose [*Hungr*, 1995; *Walton et al.*, 2007; *Mangeney et al.*, 2010]. This is particularly the case for larger rolling particles [*Zhou et al.*, 2001]. We hypothesize that a moving granular flow is more dilated in lower gravity, so that friction is lower and the dynamic angle of repose decreases with decreasing gravity.

## 2. Methods and Materials

[20] The methodology was to create confined granular avalanches during parabolic flights in a dedicated aircraft and measure the angle as a function of the resultant gravitational acceleration. Under such technically challenging conditions neither contact forces nor dilation can be measured. To exclude the effects of interstitial fluid (water and air), particle size and angularity, various materials and interstitial fluids were used simultaneously in different cylinders. To assess effects of aircraft vibrations we performed the experiment in $g = 1$ in the aircraft as well as on the ground. Below we describe the aircraft and measurement equipment, the experimental setup and the image analysis procedure to extract the angles from the digital video and the measured accelerations.

### 2.1. Aircraft and Flight Data Collection

[21] The aircraft is a Cessna Citation 550 II PH-LAB (Figure 2), a research aircraft owned and operated jointly by the National Aerospace Laboratory NLR and Delft University of Technology, Faculty of Aerospace Engineering. The platform is equipped with a partial-gravity flight director designed at Delft University of Technology to maximize the accuracy of the parabolic flights at arbitrary $g$ within operating and safety limits of the aircraft.


**Figure 2.** The Cessna Citation aircraft of Delft University of Technology and the Dutch National Aerospace Laboratory used for the parabolic flights.

[22] An accurate three axis accelerometer and ring laser gyro system recorded all trajectory parameters at 50 Hz, including relative accelerations in flight direction ($a_x$), transversely ($a_y$) and vertically ($a_z$) with respect to the aircraft. These accelerations are relative to $g_e$ when the aircraft is at rest in horizontal position so that $a_x = a_y = 0$. The magnitude of the relative gravitational acceleration $g_{eff}$ was calculated as:

$$g_{eff} = \sqrt{a_x^2 + a_z^2} \tag{1}$$

whereby transverse accelerations $a_y$ were neglected because we have two-dimensional granular flows in narrow cylinders. The $a_y$ were twice as small as $a_x$, more than an order of magnitude smaller than $a_z$.

[23] To maintain the correct velocity for constant $g_{eff}$, the aircraft tilt relative to the $g$-vector varies during the parabola. The angle $\phi$ (in °) between aircraft and $g$ is calculated as:

$$\phi = \frac{360}{2\pi} \arctan \frac{a_x}{-a_z} \tag{2}$$

[24] A time series of about 7 minutes data during slow descend (between 92.1 and 98.9 minutes time on the acceleration record) was analyzed to study the noise and fluctuations of the three acceleration components and the net $g_{eff}$. Spectral analysis was done by the power spectral density estimate via Welch's method, using window sizes of 400, 2000 and 10000, combined in one plot to show temporal structure at different timescales. Furthermore the spectral power was converted to amplitude expressed in $g_{eff}$ and the frequency expressed as period to allow direct interpretation (Figure 3).

[25] The spectral analysis demonstrated that the $a_x$ and $a_y$ components had no structure except noise (red wall climber) at 10 Hz and faster (Figure 3). The $a_z$ and $g_{eff}$ also had this red noise but there a clear spectral peak was observed at 0.05 Hz (20 s period). The low-frequency fluctuations are attributed to aircraft movement due to turbulence and hysteretic pilot-aircraft interaction. The high-frequency is explained as noise in the instruments and electronics and perhaps interference between the two jet engines. The effect of the high-frequency noise on the experimental results will be assessed by comparing the results of the 1 $g$ flight experiments to control experiments on the ground.

[26] To remove the noise, the 50 Hz acceleration time series was median filtered with a window size of 1 s before calculating equations (1) and (2). A binary signal was recorded and shown as a signal LED on the experimental setup when the required $g$-level was obtained within a tolerance of ±0.01. For each parabola equations (1) and (2) were applied to the period of accepted $g$-levels. Averages and [10,90] percentiles of $g$-levels and $\phi$ (Figure 4) were used to select acceptable parabolas for further analysis.

### 2.2. Experimental Setup and Granular Materials

[27] The basic idea is to fill half of a cylinder with a transparent sidewall with granular material and then rotate it continuously at a constant angular velocity in the discrete avalanching regime. To cover the parameter space of particle diameter, roughness and interstitial fluid a fixed array of nine cylinders was used.

[28] The rotating cylinder system was here preferred over a sand pile or funnel for a theoretical and a practical reason. A continuous flow in a pouring setup would not allow measurement of the static angle of repose, whereas a granular material in a slowly rotating cylinder exhibits both static and dynamic phases. The angular velocity was chosen at 0.14 RPM to optimize the number of avalanches per parabola but remain in the linear avalanche slope regime rather than in the cascading S-shaped regime [*Brucks et al.*, 2007]. Furthermore, the cylinder can remain closed so that there is no risk of spilling light granular material and water in the experimental aircraft. Moreover, it can continuously be rotated without having to empty and reload the measurement volume, so that no valuable time is lost during the mission.

[29] Nine cylinders were built of PVC with a perspex front, with a diameter of 0.210 m and a height of 0.060 m. The height was a compromise: the angle of repose is affected by wall friction for large ratios of particle diameter and cylinder height [*Dury et al.*, 1998; *Zhou et al.*, 2001], but the avalanches should remain two-dimensional with the entire front moving at similar velocity rather than forming a tongue-shaped avalanche flanked by immobile particles [*Kleinhans*, 2005a]. The cylinders were mounted on the frame (Figure 5) and driven at the same rate by a pulse width controlled three-phase brushless electromotor.

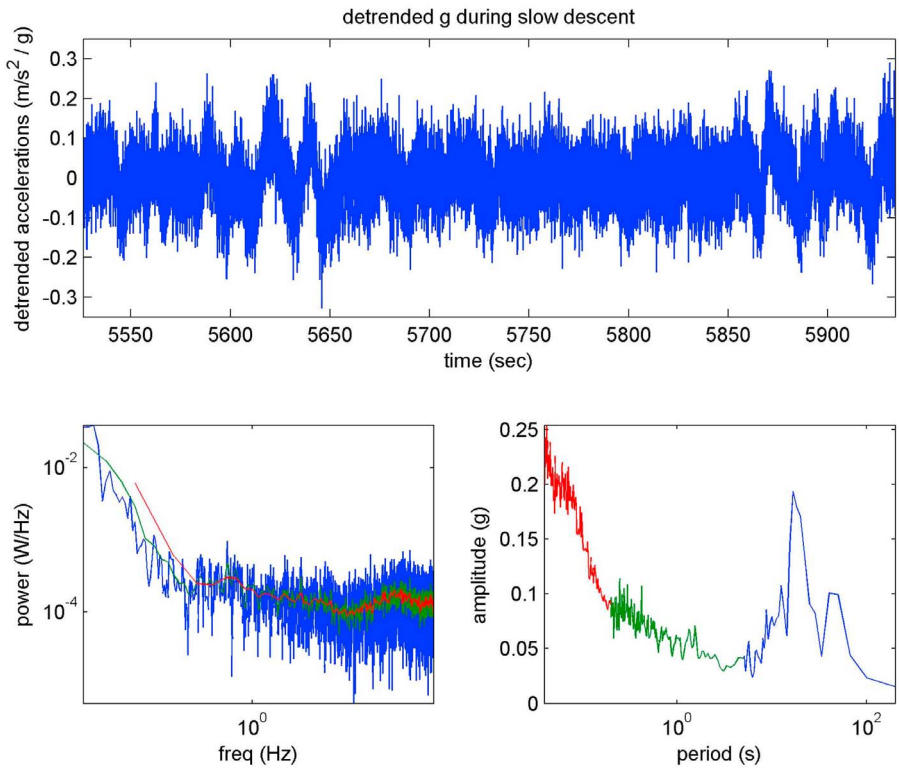


**Figure 3.** Spectral analysis of net g-vector due to aircraft motion. Red wall climber is attributed to electronics noise or engine interference noise. The spectral peak at 20 s is attributed to turbulence and hysteretic aircraft response to pilot feedback.

[30] The cylinders were filled with granular materials (Table 1), where the top row, with the lighter air-filled cylinders, refers to the top of the frame. Both sand and glass beads have a specific density of 2.65 (water has 1, air has about 0.001) and a porosity of about 30–40%. The materials were chosen to range from small to large size ranging from Stokes to inertial settling regimes in water [*Dietrich*, 1982], from rounded glass beads (ballotini) to angular fluvial sand, and with air and water as interstitial fluid. The cylindrical wall was coated with the same granular material for each cylinder. The cylinders were prepared at 70% humidity of the air so we cannot exclude the possibility of formation of microscopic water pockets in the dry cases.

[31] The rationale for performing experiments in both water and air is not merely that loose granular materials avalanche in both environments, but also that the subaqueous experiments have negligible electrostatic force effects and can also not be affected by surface tension of microscopic water pockets in the dry cases. However, fluid friction is present in the subaqueous systems, and it varies with particle diameter squared depending on the Stokes number, which describes the relative effects of grain inertia and fluid viscous effects [*Allen*, 1965, 1972; *Dietrich*, 1982; *Courrech du Pont et al.*, 2003].

[32] The materials were selected based on the phase diagram by *Courrech du Pont et al.* [2003, Figure 3]. This diagram defines three regimes: the viscous limit regime, inertial limit regime and free-fall regime. This is based on two variables: $r$, which is the material density $\rho_s$ relative to fluid density $\rho_w$: $r = (\rho_s/\rho_w)^{1/2}$, and the Stokes number $St$, here calculated as the ratio of the characteristic time to reach the viscous limit velocity, and the characteristic time of free falling over a distance equal to the particle diameter:

$$St = \frac{\rho_s D^2}{18\eta}\sqrt{\frac{(\rho_s - \rho_w) g \sin\theta}{2\rho_s D}} \tag{3}$$

where $\eta$ = fluid viscosity and $\sin\theta$ = angle of repose.

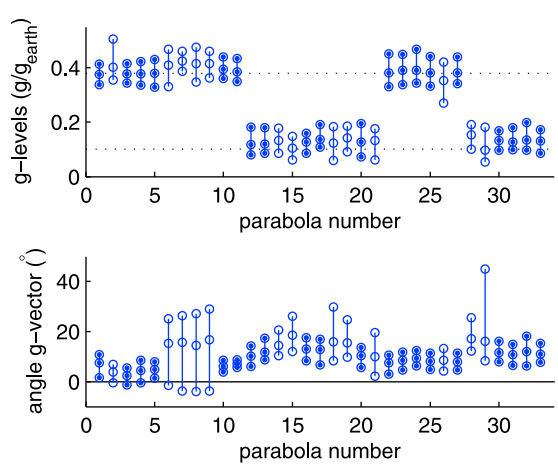


**Figure 4.** Mean, 10% and 90% percentiles of (top) g-levels and of (bottom) aircraft angle relative to the acceleration vector in each parabola. Rejected data have open symbols.

**Figure 5.** The experimental setup. Cylinders are 0.21 m in diameter. Cameras are located to the left.

[33] Stokes numbers were calculated for 0.1, 0.38 and 1 *g* (Table 1) assuming a fluid viscosity of $1.0 \times 10^{-3}$ Ns/m$^2$ and air viscosity of $1.8 \times 10^{-5}$ Ns/m$^2$ at room temperature, and an angle of repose of 25° for glass beads and 40° for angular particles. For translation to Martian conditions the air viscosity of a carbon dioxide atmosphere at the freezing point for water is about 75% of the value for standard air at room temperature. For comparison, the transition from viscous to inertial regime in water takes place at about $St$ = 3–4, the transition from viscous to free-fall regime in air takes place at $St$ = 10 and the transition from inertial to free-fall regime for $St$ > 10 takes place at $r$ = 4 [*Courrech du Pont et al.*, 2003]. As a result, in air all materials are always in the free-fall regime but approach the viscous regime for the 0.2 mm material, all materials of 0.6 mm in water are in the viscous regime but approach the inertial regime for the highest gravity, and all materials of 2 mm and larger in water are always in the inertial regime but approach the viscous regime transition in lower gravity. *Courrech du Pont et al.* [2003] found that the difference between static and dynamic angle of repose only depended on Stokes number for $St$ < 10, where it decreased with decreasing $St$. The selected materials allow the isolation of the effect of gravity on the angles of repose independently of the dependence on Stokes number.

[34] Furthermore, preliminary laboratory experiments indicated that interstitial fluid dynamics were very important for the static angle of repose in very fine granular materials, including the 0.2 mm glass beads and sand in water. A granular material transitioning from static to mobile will have to dilate, which means that fluid has to enter the interstices. For fine materials this takes significant time so that the material oversteepens up to 90° [*Van den Berg et al.*, 2002]. The dynamic angle is unaffected given enough time for the flow to occur. As the duration of such avalanches far exceeds the duration of reduced gravity in a parabolic flight, we did not include subaqueous fine sediments.

### 2.3. Image Analysis

[35] Two High Definition (HD) consumer video cameras (Canon HF10E) recorded the avalanching process. The cameras were mounted on a small frame on the opposite side of the cabin. The high-frequency measurement of angles of the aeroplane relative to the 'gravity' force vector and effective 'gravitational' acceleration by the flight director instruments were synchronized with the video by LED event markers on the frame. The camera settings were non-interlaced, 25 Hz, nearly lossless compression, an image aspect ratio of 16:9 and a resolution of 1440 × 1080 pixels. The HD cameras were started simultaneously before the onset of each parabola and terminated afterwards. The entire video of each parabola was analyzed and the relevant time period for low gravity selected afterwards by synchronization to the event marker LEDs. The middle three cylinders were imaged by both cameras as a check on the analysis.

[36] Each image of the movies was analyzed as follows, to yield a time series of angle of the sediment at 25 Hz. A circular mask was created within the rim of each cylinder, so that only sediment and interstitial fluid remained. This image was thresholded and binarized. Boundaries of the sediment were identified and the circle segment was removed to yield a line following the fluid-sediment interface. Robust regression was applied to calculate the angle of this line. The robust regression algorithm uses iteratively reweighted least squares with a bisquare weighting function. Median-filtering of the time series was required to remove spikes caused by changing lighting during the parabolic trajectory of the aircraft.

[37] The resulting time series showed the gradual steepening of the granular material slope due to cylinder rotation and the sudden decrease of the slope as the material avalanched (Figure 6). The measured angles of repose of the granular materials were corrected for the angle $\phi$ of the aircraft with the $g_{eff}$ vector (Figure 6). Neither the slight misalignment of the cameras relative to the experimental frame nor the barrel distortion of the camera optics were corrected, as the objective was to find angle differences

**Table 1.** Granular Material and Interstitial Fluid for the Rotating Cylinders[a]

| | Cylinder Column 1 | Cylinder Column 2 | Cylinder Column 3 |
|---|---|---|---|
| Cylinder row 1 | 2.4 mm gravel in air<br>$St$ = 530, 1033, 1675 | 0.21 mm sand in air<br>$St$ = 13, 26, 42 | 0.2 mm glass beads in air<br>$St$ = 11, 21, 34 |
| Cylinder row 2 | 2 mm glass beads in air<br>$St$ = 327, 637, 1033 | 0.6 mm sand in air<br>$St$ = 66, 129, 209 | 0.6 mm sand in water<br>$St$ = 0.9, 1.8, 3.0 |
| Cylinder row 3 | 2.4 mm gravel in water<br>$St$ = 7.5, 14.6, 23.7 | 2 mm glass beads in water<br>$St$ = 4.6, 9.0, 14.6 | 0.6 mm glass beads in water<br>$St$ = 0.8, 1.5, 2.4 |

[a]Order same as in Figure 5. Stokes numbers are calculated for 0.1, 0.38 and 1 *g*. For comparison, the transition from viscous to inertial regime in water takes place at about $St$ = 3–4 and the transition from viscous to free-fall regime in air takes place at $St$ = 10 [*Courrech du Pont et al.*, 2003].

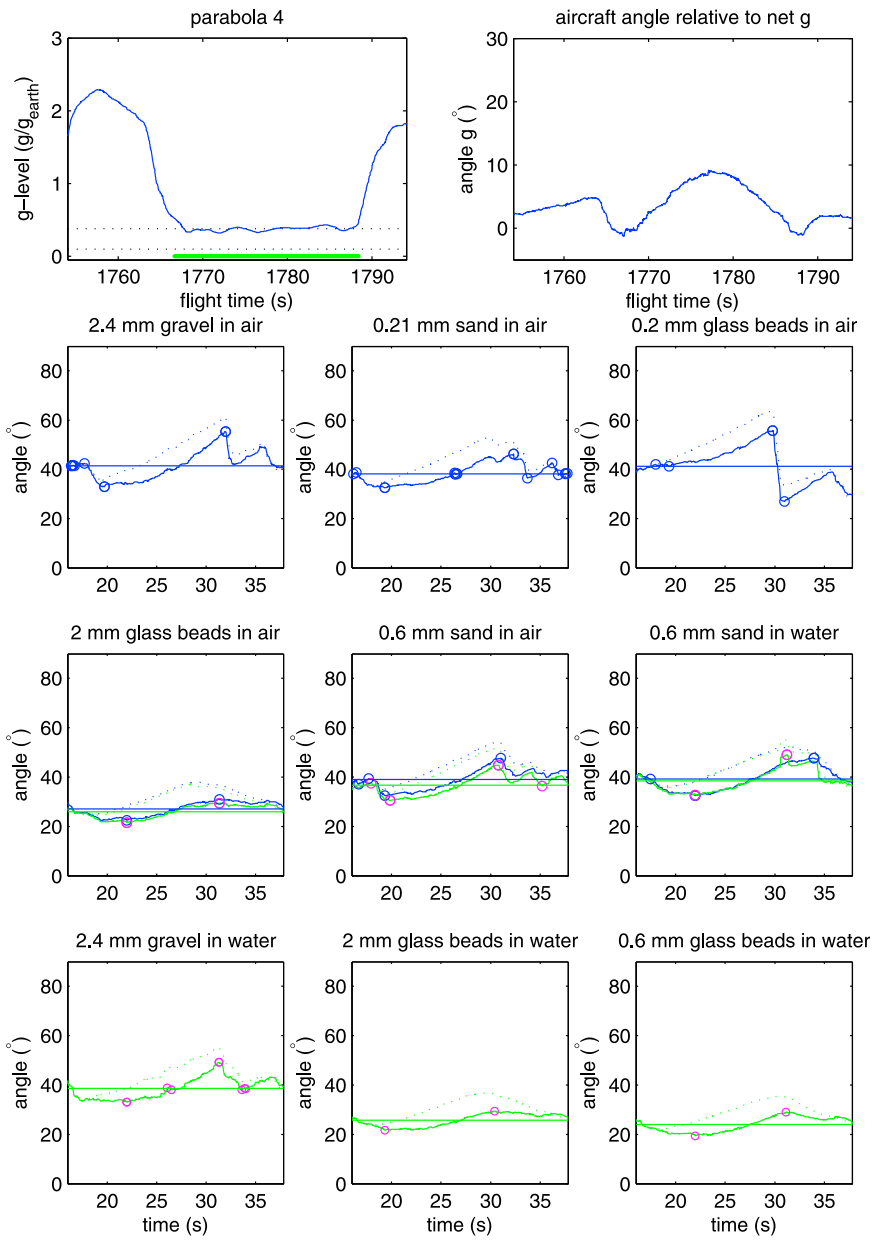


**Figure 6.** Example data of one parabola. Dotted lines indicate sediment angles before correction with the aircraft angle relative to the acceleration vector. Circles indicate unfiltered static and dynamic angles of repose. Blue lines were derived from the top camera and green lines from the bottom camera.

between the g-levels rather than absolute values. The maximum systematic errors of the angles due to the barrel distortion are estimated as ±2°.

[38] The steepest angle is interpreted to be the static angle of repose and the gentlest angle the dynamic angle of repose, unless the movie shows continuous avalanching. These were calculated by calculating the average of the time series, identifying the zero crossings and calculating the local maximum or minimum between the times of crossing (circles in Figure 6) [see also *WAFO Group*, 2000; *Brodtkorb et al.*, 2000]. The duration of the parabolas was just sufficient to identify at least one avalanche in each drum so that it was certain that a static and a dynamic angle were measured. This was checked with a long-duration time series at $g = 1$ in the hangar (Figure 7). Further data reduction was done by calculating the [10,90] percentiles of the dynamic and the static angles, respectively.

## 3. Results

[39] Our main result is surprising: for decreasing gravity, the static angle of repose increases while the dynamic angle of repose decreases for all materials (Figures 8 and 9). The increase of the static angle of repose is about 5° with decreasing gravitational acceleration (from 1 to 0.1 $g$), whereas the dynamic angle decreases with about 10°. The difference, called dilation angle, therefore increases roughly an order of magnitude. Consequently, the avalanche size increases strongly with decreasing $g$. The time-averaged angle of repose decreases slightly with decreasing $g$.

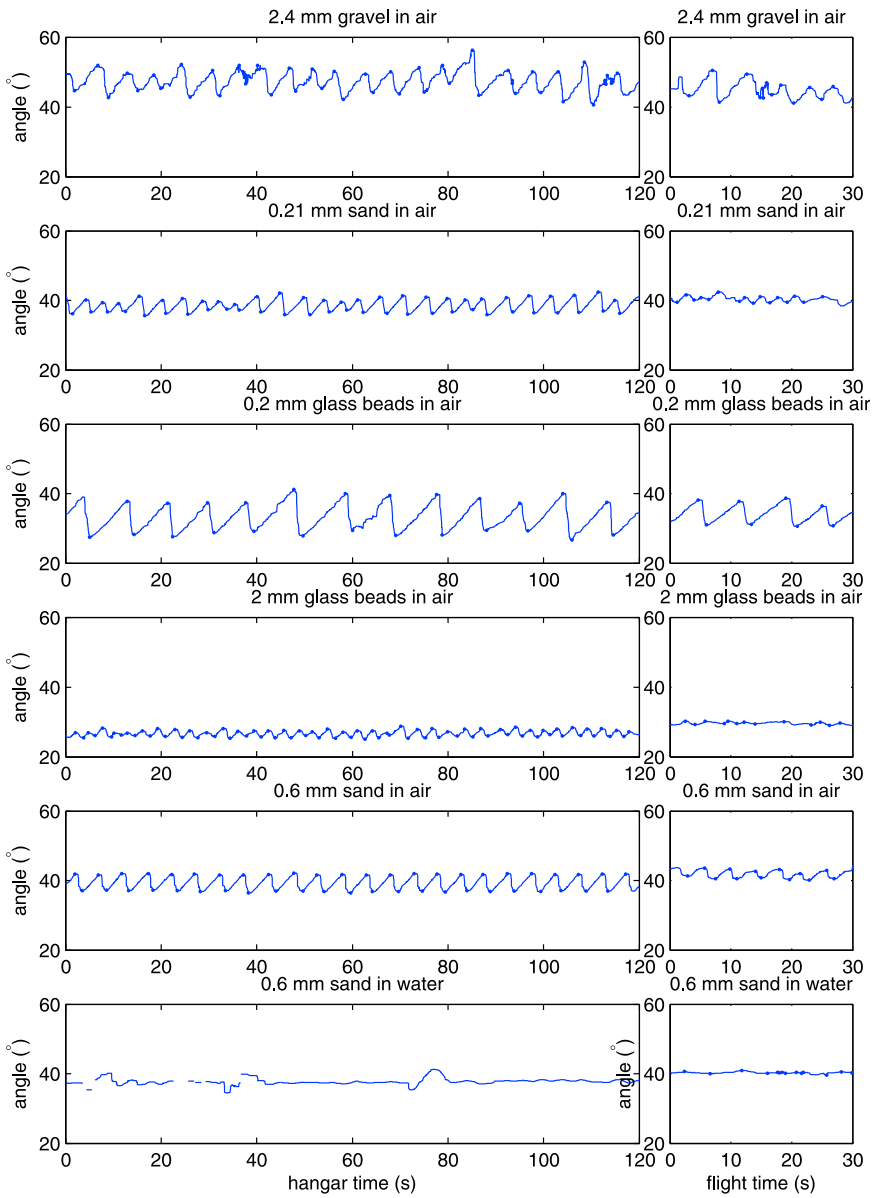


**Figure 7.** Comparison of time series for 1 *g* (left) in the hangar and (right) in flight. The median angle may be vertically displaced because the camera was remounted in the hangar, but the difference with static and dynamic angles of repose has no bias. Possibly the slightly smaller differences for the flight cases are caused by aircraft vibration.

[40] The effect of particle rounding was considerable but unsurprising. Angular materials (the gravel, fine and medium sands) had time-averaged angles of about 40° and rounded materials (glass beads) about 25° for all *g* except the finest glass beads in air.

[41] The interstitial fluid hardly affected the main results: the angles of repose for water and air were similar despite the large difference in Stokes numbers (Table 1). Also particle size hardly made a difference, which rules out effects of particle momentum, fluid drag on settling particles and on the avalanches, and rules out interstitial fluid dynamics as a significant effect on the angle of repose. However, the avalanches in water were much slower than in air as can be expected based on fluid drag.

[42] The effect of wall friction may have caused a small systematic increase of all measured angles, but does not affect the differences between levels of gravity or particle sizes. The fact that an order of magnitude difference in particle size relative to cylinder height does not give a significantly different angle of repose suggests that wall friction is negligible for the present measurement accuracy.

[43] The 0.2 mm glass beads in air behaved cohesively. The other granular materials did not show a significant difference between the static and dynamic angles of repose in air and in water, which indicates that electrostatic effects and capillary effects of microscopic water pockets are negligible in all experiments except the 0.2 mm glass beads. These glass beads clung to, and propagated along the transparent front of the cylinder by static electricity. There is

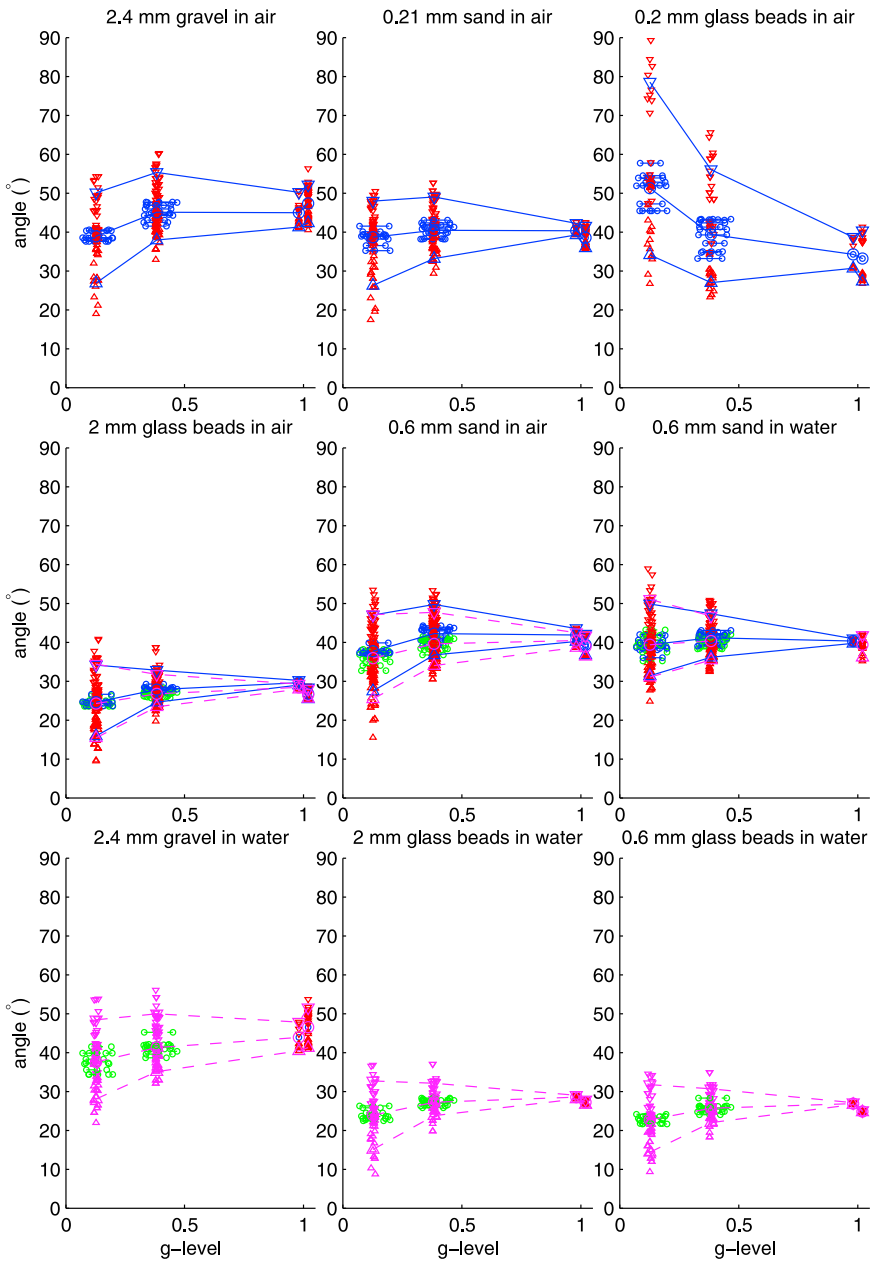


**Figure 8.** Time-averaged angle, static angle of repose and dynamic angle of repose for each sediment. Individual observations indicated by triangles. Values plotted at 0.98 $g$ are control measurements in the flight at 1 $g$ and values plotted at 1.02 $g$ are control measurements on the ground at 1 $g$ (uncorrected for camera and setup angle). Maximum is calculated as 90% percentile from static angles (see Figure 6) and minimum is calculated as 10% percentile from dynamic angles.

a slight increase of the angles for the 2 mm glass beads in air relative to that in water, but the gravel and the 0.6 mm sand shows the opposite (weak) trend so it must be doubted that this is significant. Also the 0.2 mm sand did not seem to be affected by electrostatic or capillary effects.

[44] The effect of aircraft vibrations on the trend appears negligible. Although is possible that the vibration caused some minor bias toward lower angles of repose (both static and dynamic) at lower effective gravity, we could not resolve such an effect. The control experiments in the aircraft at $g = 1$ and in the hangar at $g = 1$ (Figure 7) show similar results with differences in average angle that are well explained by the systematic errors in camera angle as the camera was mounted in a different manner than in the aircraft. It is possible that the small reduction in difference between static and dynamic angles is due to aircraft vibration. Accelerations due to aircraft vibration would decrease the angle of repose as the avalanching is fast whereas the build-up of the slope is slow, and would affect the low $g$ the most assuming that the accelerations due to the vibrations are independent of $g_{eff}$. However, the data show no consistent decrease of the angle. On the contrary, the static angle of repose, which may be the most sensitive, increases with decreasing $g$. This is in agreement with *Evesque and*

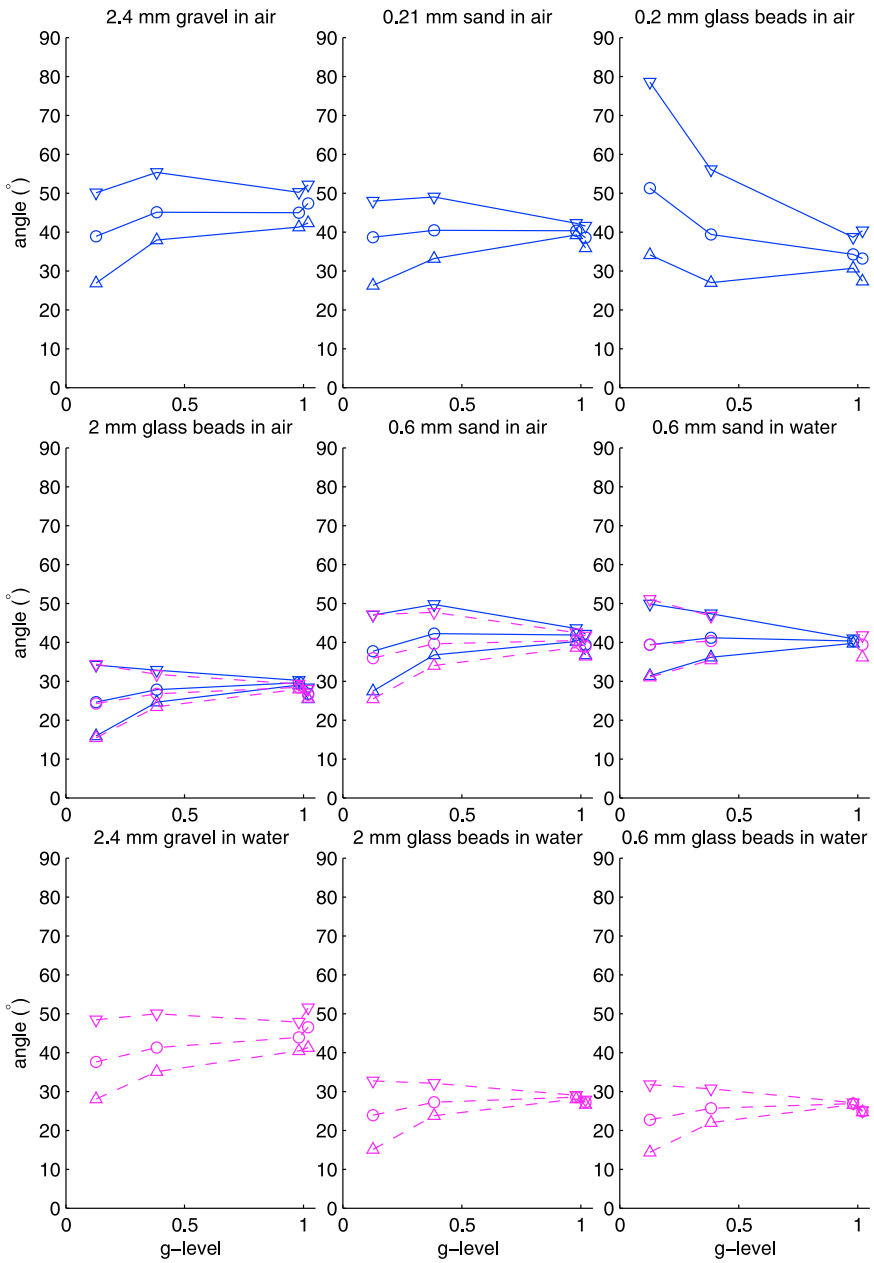


**Figure 9.** Time-averaged angle, static angle of repose and dynamic angle of repose for each sediment. Same as Figure 8 without data. Maximum is calculated as 90% percentile from static angles (see Figure 6) and minimum is calculated as 10% percentile from dynamic angles.

*Rajchenbach* [1989] who show that accelerations due to vibration must be of the same order as the gravitational acceleration to move the granular material. It is conceivable that the slight flattening of the curves of static angle of repose toward lower $g$ is due to the vibrations but the effect is smaller than measurable with this setup.

## 4. Discussion

### 4.1. Test of Hypotheses and Comparison to Other Data

[45] The experimental data show a novel result: the static angle of repose increases while the dynamic angle of repose decreases in lower gravity. This is in direct disagreement with a large body of work that assumes the angles of repose to be independent of gravity. An immediate effect of the larger dilation angle is that the avalanches in the experiments may be larger and occur less often than in terrestrial gravity. Although only three $g$-levels were imposed, the data indicate a stronger than linear relation between dilation angle and gravity. Furthermore, the results indicate that an important assumption in models of many morphological phenomena, also at much lower slopes, is violated. If our experimental results have general validity then the consequence is that many such model results and interpretations of measurements must be revisited (see section 1 for examples).

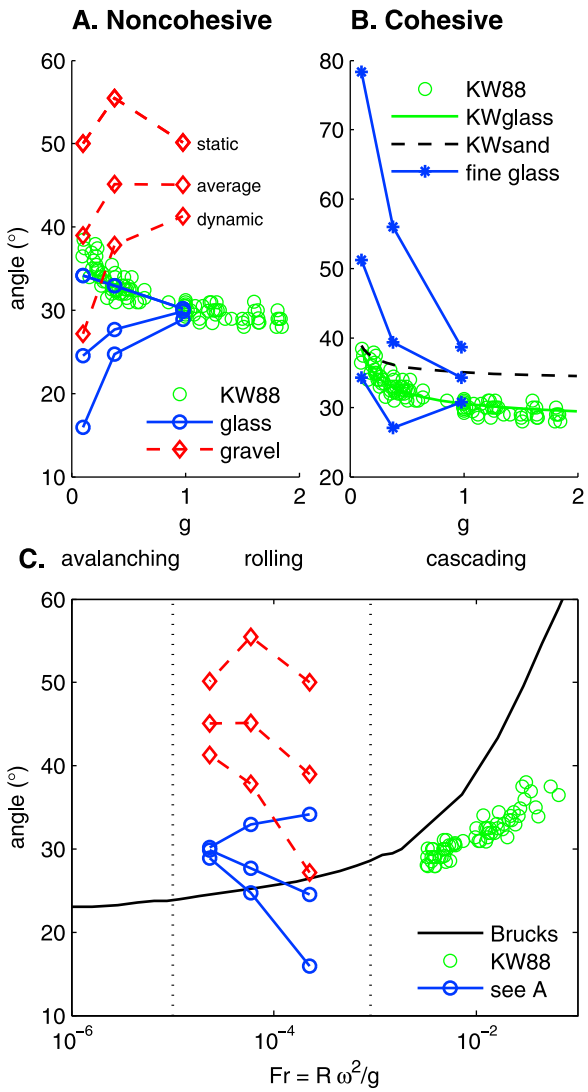


**Figure 10.** Comparison to data from literature. (a) Comparison of angular 2.4 mm gravel and rounded 2 mm glass beads in air with 1.35 mm glass bead data of *Klein and White* [1990], 'KW90'. (b) Comparison of 0.2 mm glass beads in air, showing cohesive behavior, with data and fitted functions of *Klein and White* [1990] for 1.35 mm glass beads (data shown) and 0.4 mm sand (data not given in source). (c) Comparison of flow regimes in our data [*Klein and White*, 1990] and solid curve from *Brucks et al.*'s [2007, Figure 3] data.

[46] The two hypotheses developed in the introduction are that the static angle of repose increases with decreasing gravity whereas the dynamic angle of repose decreases with decreasing gravity. The data confirm both hypotheses. First, the static angle of repose increases with decreasing gravity, perhaps because packing density of large static particles is independent of gravity. Second, the dynamic angle of repose decreases with decreasing gravity, perhaps because a moving granular flow is more dilated in lower gravity, so that friction is lower and run-out continues longer. These hypotheses obviously required further investigation by numerical modeling.

[47] Our results contradict those of *Klein and White* [1990]; the relation between angle of repose and gravity are opposed (Figures 10a and 10b). On the other hand, our data are confirmed by Hele-Shaw cell experiments done during the same flights (S. J. de Vet, manuscript in preparation, 2011), and by a limited data set from drop-tower experiments [*Blum*, 2010], which showed lower angles and larger run-out lengths. *Walton et al.* [2007] reanalyzed the data and movies of *Klein and White* [1990], revealing an important difference with our setup: their experiments were in the continuous avalanching mode, contrary to ours that had discrete avalanching. Hence the data of *Klein and White* [1990] represent the dynamic angle of repose only.

[48] Our results are incomparable to data collected in centrifuges (Figure 10c). Not only are the trends are opposed, also the avalanching regime is different. The data of *Klein and White* [1990] and *Brucks et al.* [2007] are mostly in the continuous avalanching ('rolling') and cascading regimes, whereas ours were observed to be in the discrete avalanching regimes. Some rotating drum experiments with discrete avalanching confirm that the difference between static and dynamic angle of repose increases for lower rotation rates [*Dury et al.*, 1998]. Continuous avalanching and cascading are both conditions that may occur in a rotating drum at higher speeds, where effective gravity is increased by the rotation. Avalanches on planetary surfaces are expected to be discrete events, so we believe our findings to be representative for those conditions.

[49] *Walton et al.* [2007] suggest that the 1.35 mm glass beads of *Klein and White* [1990] started to show cohesive behavior at low gravity. In cohesive material such as fine powder, bulk deformation takes place with large critical angles, clumping and collapse of steep structures, but this behavior disappears when increasing gravity overwhelms the cohesive forces, as in experiments done with rotating drums in a centrifuge with $12.5 < g < 1200$ [*Walton et al.*, 2007]. By extrapolating this data to low $g$, cohesion becomes relatively more important in granular materials that are noncohesive under terrestrial gravity. However, our particles and those of *Klein and White* [1990] are much larger than the powders of *Walton et al.* [2007]. Indeed, we do neither expect nor observe cohesive behavior in our experiments except with the smallest particles in air. It is more likely that the cohesive behavior is due to static electricity or capillarity. We therefore suggest that the *Klein and White* [1990] data is not representative for avalanches on planetary surfaces. The effects were excluded in the subaqueous experiments, which gave very similar results to the subaerial experiments so that the data presented here are not significantly affected by static electricity or capillarity. Neither did the fluid cause the increasing dilation angle for decreasing gravity; on the contrary, as gravity decreased the Stokes number decreased, which should have caused a decrease in dilation angle [*Courrech du Pont et al.*, 2003].

### 4.2. Consequences for Surface Morphology of Terrestrial Moons and Planets

[50] Gully alcove slopes measured on Mars were found to range mostly between 24–30° and a maximum of 42° [*Dickson et al.*, 2007; *Parsons and Nimmo*, 2010]. These angles are generally lower than expected for coarse angular

material, which was explained by lubrication and even transport by meltwater. However, our findings suggest that the range found on Mars may also be explained by the significant reduction of the dynamic angle of repose under lower gravity. A different feature is the slope streak associated to triangular scars [*Gerstell et al.*, 2004; *Kreslavsky and Head*, 2009; *McEwen et al.*, 2006]. These sometimes have low slopes but in general have slope angles between 28–38°, which agrees well with the dynamic angle of repose of the experimental angular material under reduced gravity. This suggests that at least some of the cases did not require lubrication to form.

[51] The angle of repose as an empirical friction parameter is important in models of a large range of morphological phenomena at much lower slopes. The experimental results therefore suggest that these phenomena would also be affected by gravity. This includes, for instance, the threshold for fluvial and aeolian sediment transport at low gradient, which could imply larger transport rates and earlier entrainment than on Earth [*Kleinhans*, 2005b]. Such predictions are hard to test in practice as detailed material properties on other planetary bodies are very hard to constrain. Furthermore, the reduced angle of dynamic repose under lower gravity could perhaps explain the larger run-out length of Martian landslides compared to terrestrial cases [*Lucas and Mangeney*, 2007].

[52] Perhaps in some conditions we can use the predictions inversely to predict material properties. For instance, the steepest angle at the subaqueous foreset of the Nepenthes delta on Mars is 31° [*Kleinhans et al.*, 2010]. We may assume that the surface sediment of Mars is extremely coarse-grained with median sizes of the order of 0.5 m diameter, and is angular because of the proximity of the source, which is the impact-related megaregolith [*Kleinhans*, 2005b; *Golombek et al.*, 2008]. On Earth, this sediment would have a very large dynamic angle of repose and even larger static angle. The 2.4 mm gravel in water of our experiments has a dynamic angle of about 40° in terrestrial gravity, but a lower angle of about 35° in Martian gravity. For the Nepenthes delta this value agrees well. Backward analysis of landslides through modeling has been used to infer rheological properties, which was then used to infer the role of interstitial water, carbon-dioxide or brines and the climate consequences on Mars [*Harrison and Grimm*, 2003; *Lucas and Mangeney*, 2007; *Pirulli and Mangeney*, 2008; *Kreslavsky and Head*, 2009; *McEwen et al.*, 2006]. However, the increasing dilation angle for reduced gravity renders reinterpretation necessary; perhaps the Martian flows can equally well be reproduced with less fluid.

[53] The results may also have implications for asteroids, perhaps for granular avalanches on craters in very low gravity. As the experimental results at 0.1 $g$ may have been affected by vibration, it is hard to predict whether the slopes will be higher or lower at reduced gravity. The angle of repose is also relevant for predictions of the shape of asteroids. A model study on the shape of asteroids composed of loose granular material with self-gravity at the angle of repose reproduced the form of the Saturnian moon Atlas and a NEO but also produced very different shapes for higher angles of repose [*Minton*, 2008]. Assuming that the dynamic angle of repose is relevant for a movable pile of particles, the lower dynamic angle of repose for lower gravity could predict different asteroid shapes. In lower gravity cohesive forces may also become relatively more important, which affects granular movement, asteroid shape and the inference of the size and nature of the granular material that composes asteroids [*Scheeres et al.*, 2010]. Our data suggest that asteroids with $g \approx 0.02$ could have static slope angles of repose up to 50° and dynamic angles of repose less than 20° for loose angular granular material.

[54] Finally, future drilling, robot propagation and processing plants of granular material on the Moon or Mars require intimate understanding of granular materials [*Anderson et al.*, 2009]. The increased static angle of repose under reduced gravity implies that it will be more difficult to drill or move granular materials than on Earth.

## 5. Conclusions

[55] Angles of repose of granular material depend on gravity: in low-gravity, the static angle of repose increases and the dynamic angle of repose decreases, leading to larger-volume avalanches. This contradicts earlier results and common understanding that the angles are independent of gravity. The findings are valid for particle sizes between 0.2–2.4 mm, smooth spherical to angular particles, and with air and water as interstitial fluids. At planetary surfaces, the lower dynamic angles of repose are expected to be preserved in deposits and the higher static angles of repose in the erosional scarps on the steepest slopes. As the angle of repose functions as a parameter in models for a wide range of morphological phenomena occurring at much gentler slopes, the effect of the dependence on gravity on these phenomena should be considered.

[56] **Acknowledgments.** The project was supported by the Netherlands Space office (grants SRON PB 09/001 and 2009-0142/TVD) and the Young Academy of the Royal Netherlands Academy of Arts and Sciences. The authors contributed as follows: M.G.K. and H.M. designed the experiment, H.M. built the experimental setup, M.G.K. did experiments, analyzed the data and prepared the manuscript, S.J.d.V. (PI) initiated the project and conducted complementary experiments with bidisperse materials in a Hele-Shaw cell, A.C.i.t.V. was co-designer of the microgravity flight director and pilot, and F.N.P. was flight engineer. Flight safety of the instrumentation was assessed by the National Aerospace Laboratory (NLR). We gratefully acknowledge support by Henk Lindenburg, NLR and TU Delft technicians in the hangar and technicians in the NLR workshop in Amsterdam.

## References

Allen, J. (1965), Sedimentation to the lee of small underwater sand waves: an experimental study, *J. Geol.*, *73*, 95–116.

Allen, J. (1970), The avalanching of granular solids on dune and similar slopes, *J. Geol.*, *78*, 326–351.

Allen, J. (1972), Intensity of deposition from avalanches and the loose packing of avalanche deposits, *Sedimentology*, *18*, 105–111.

Allen, J. R. L., and M. R. Leeder (1980), Criteria for the instability of upper-stage plane beds, *Sedimentology*, *27*, 209–217.

Anderson, R., et al. (2009), Particle transport and distribution on the Mars Science Laboratory mission: Effects of triboelectric charging, *Icarus*, *204*, 545–557, doi:10.1016/j.icarus.2009.07.006.

Bagnold, R. (1951), The movement of a cohesionless granular bed by fluid flow over it, *Brit. J. Appl. Phys.*, *2*, suppl.1, 29–34.

Bart, G. (2007), Comparison of small lunar landslides and martian gullies, *Icarus*, *187*, 417–421.

Blum, J. (2010), Astrophysical microgravity experiments with dust particles, *Microgravity Sci. Technol.*, *22*, 517–527, doi:10.1007/s12217-010-9236-3.

Boutreux, T., H. Makse, and P.-G. D. Gennes (1998), Surface flows of granular mixtures: Iii. canonical model, *Eur. Phys. J. B*, *9*, 105–115.

Brodtkorb, P., P. Johannesson, G. Lindgren, I. Rychlik, J. Rydén, and E. Sjö (2000), WAFO: A Matlab toolbox for the analysis of random waves and loads, in *Proceedings of the 10th International Offshore and Polar Engineering Conference, ISOPE, Seattle, USA*, edited by J. S. Chung et al., vol. 3, pp. 343–350, ISOPE, Seattle, Wash.

Brucks, A., T. Arndt, J. Ottino, and R. Lueptow (2007), Behavior of flowing granular materials under variable g, *Phys. Rev. E*, *75*, 032301.

Carrigy, M. (1970), Experiments on the angles of repose of granular materials, *Sedimentology*, *14*, 147–158.

Chuang, F., and R. Greeley (2000), Large mass movements on Callisto, *J. of Geophys. Res.*, *105*(E8), 20,227–20,244.

Courrech du Pont, S., P. Gondret, B. Perrin, and M. Rabaud (2003), Granular avalanches in fluids, *Phys. Rev. Lett.*, *90*(4), 44301.

Dickson, J., J. Head, and M. Kreslavsky (2007), Martian gullies in the southern mid-latitudes of Mars: evidence for climate-controlled formation of young fluvial features based upon local and global topography, *Icarus*, *188*, 315–323, doi:10.1016/j.icarus.2006.11.020.

Dietrich, W. (1982), Settling velocity of natural particles, *Water Resour. Res.*, *18*(6), 1615–1626.

Dundas, C., A. McEwen, S. Diniega, and S. Byrne (2010), New and recent gully activity on Mars as seen by HiRISE, *Geophys. Res. Lett.*, *37*, L07202, doi:10.1029/2009GL041351.

Dury, C., G. Ristow, J. Moss, and M. Nakagawa (1998), Boundary effects on the angle of repose in rotating cylinders, *Phys. Rev. E*, *57*(4), 4491–4497.

Evesque, P., and J. Rajchenbach (1989), Instability in a sand heap, *Phys. Rev. Lett.*, *62*(1), 44–46.

Gerstell, M., O. Aharonson, and N. Schorghofer (2004), A distinct class of avalanche scars on Mars, *Icarus*, *168*, 122–130.

Golombek, M. P., et al. (2008), Size-frequency distributions of rocks on the northern plains of Mars with special reference to Phoenix landing surfaces, *J. Geophys. Res.*, *113*, E00A09, doi:10.1029/2007JE003065.

Goujon, C., B. Dalloz-Dubrujeaud, and N. Thomas (2007), Bidisperse granular avalanches on inclined planes: a rich variety of behaviors, *Eur. Phys. J. E*, *23*, 199–215, doi:10.1140/epje/i2006-10175-0.

Harrison, K., and R. Grimm (2003), Rheological constraints on martian landslides, *Icarus*, *163*, 347–362, doi:10.1016/S0019-1035(03)00045-9.

Heldmann, J., and M. Mellon (2004), Observations of martian gullies and constraints on potential formation mechanisms, *Icarus*, *168*, 285–304, doi:10.1016/j.icarus.2003.11.024.

Hungr, O. (1995), A model for the runout analysis of rapid flow slides, debris flows, and avalanches, *Can. Geotech. J.*, *32*, 610–623.

Jop, P., Y. Forterre, and O. Pouliquen (2006), A constitutive law for dense granular flows, *Nature*, *441*, 727–730, doi:10.1038/nature04801.

Jopling, A. (1964), Laboratory study of sorting processes related to flow separation, *J. Geophys. Res.*, *69*(16), 3403–3418.

Klein, S., and B. White (1990), Dynamic shear of granular material under variable gravity conditions, *Am. Inst. Aeronaut. Astronaut. J.*, *28*(10), 1701–1702.

Kleinhans, M. G. (2004), Sorting in grain flows at the lee side of dunes, *Earth Sci. Rev.*, *65*, 75–102, doi:10.1016/S0012-8252(03)00081-3.

Kleinhans, M. G. (2005a), Grain-size sorting in grainflows at the lee side of deltas, *Sedimentology*, *52*, 291–311, doi:10.1111/j.1365-3091.2005.00698.x.

Kleinhans, M. G. (2005b), Flow discharge and sediment transport models for estimating a minimum timescale of hydrological activity and channel and delta formation on Mars, *J. Geophys. Res.*, *110*, E12003, doi:10.1029/2005JE002521.

Kleinhans, M. G. (2010), A tale of two planets: Geomorphology applied to Mars' surface, fluvio-deltaic processes and landforms, *Earth Surf. Proc. Landforms*, *35*, 102–117, doi:10.1002/esp.1895.

Kleinhans, M. G., H. van de Kasteele, and E. Hauber (2010), Palaeoflow reconstruction from fan delta morphology on Mars, *Earth Planet. Sci. Lett.*, *294*, 378–392, doi:10.1016/j.epsl.2009.11.025.

Kreslavsky, M., and J. Head (2009), Slope streaks on Mars: A new "wet" mechanism, *Icarus*, *201*, 517–527, doi:10.1016/j.icarus.2009.01.026.

Lowe, D. (1976), Grain flow and grain flow deposits, *J. Sed. Pet.*, *46*, 188–199.

Lucas, A., and A. Mangeney (2007), Mobility and topographic effects for large Valles Marineris landslides on Mars, *Geophys. Res. Lett.*, *34*, L10201, doi:10.1029/2007GL029835.

Makse, H., R. Ball, H. Stanley, and S. Warr (1998), Dynamics of granular stratification, *Phys. Rev. E*, 58.

Malin, M. (1992), Mass movements on Venus: preliminary results from Magellan cycle 1 observations, *J. of Geophys. Res.*, *97*(E10), 16,337–16,352.

Mangeney, A., O. Roche, O. Hungr, N. Mangold, G. Faccanoni, and A. Lucas (2010), Erosion and mobility in granular collapse over sloping beds, *J. Geophys. Res.*, *115*, F03040, doi:10.1029/2009JF001462.

Mangeney-Castelnau, A., F. Bouchut, J. Vilotte, E. Lajeunesse, A. Aubertin, and M. Pirulli (2005), On the use of Saint Venant equations to simulate the spreading of a granular mass, *J. Geophys. Res.*, *110*, B09103, doi:10.1029/2004JB003161.

McEwen, A., L. Ojha, C. Dundas, S. Mattson, S. Byrne, J. Wray, S. Cull, S. Murchie, N. Thomas, and V. Gulick (2006), Seasonal flows on warm martian slopes, *Science*, *333*, 740–743, doi:10.1126/science.1204816.

Melosh, H., and B. Ivanov (1999), Impact crater collapse, *Annu. Rev. Earth Planet. Sci.*, *27*, 385–415.

Minton, D. (2008), The topographic limits of gravitationally bound, rotating sand piles, *Icarus*, *195*, 698–704, doi:10.1016/j.icarus.2008.02.009.

Parker, G., and E. Andrews (1985), Sorting of bed load sediment by flow in meander bends, *Water Resour. Res.*, *21*(9), 1361–1373.

Parsons, R., and F. Nimmo (2010), Numerical modeling of martian gully sediment transport: testing the fluvial hypothesis, *J. Geophys. Res.*, *115*, E06001, doi:10.1029/2009JE003517.

Pirulli, M., and A. Mangeney (2008), Results of back-analysis of the propagation of rock avalanches as a function of the assumed rheology, *Rock Mech. Rock Eng.*, *41*(1), 59–84, doi:10.1007/s00603-007-0143-x.

Pohlman, N., B. Severson, J. Ottino, and R. Lueptow (2006), Surface roughness effects in granular matter: Influence on angle of repose and the absence of segregation, *Phys. Rev. E*, *73*, 031,304.

Pouliquen, O. (1999), Scaling laws in granular flows down rough inclined planes, *Phys. Fluids*, *11*(3), 542–548.

Rickenmann, D. (1999), Empirical relationships for debris flows, *Nat. Hazards*, *19*, 47–77.

Scheeres, D., C. Hartzell, P. Sánchez, and M. Swift (2010), Scaling forces to asteroid surfaces: The role of cohesion, *Icarus*, *210*, 968–984, doi:10.1016/j.icarus.2010.07.009.

Soulsby, R., and J. Damgaard (2005), Bedload sediment transport in coastal waters, *Coastal Eng.*, *52*, 673–689.

Van den Berg, J., A. van Gelder, and D. Mastbergen (2002), The importance of breaching as a mechanism of subaqueous slope failure in fine sand, *Sedimentology*, *49*, 81–95.

Vollmer, S., and M. G. Kleinhans (2007), Predicting incipient motion including the effect of turbulent pressure fluctuations in the bed, *Water Resour. Res.*, *43*, W05410, doi:10.1029/2006WR004919.

WAFO Group (2000), *WAFO-A Matlab Toolbox for Analysis of Random Waves and Loads: A Tutorial*, Math. Stat., Cent. for Math. Sci., Lund Univ., Lund, Sweden.

Walton, O., C. De Moor, and K. Gill (2007), Effects of gravity on cohesive behaviour of fine powders: implications for processing Lunar regolith, *Granular Matter*, *9*, 353–363, doi:10.1007/s10035-006-0029-8.

Wiberg, P., and J. Smith (1987), Calculations of the critical shear stress for motion of uniform and heterogeneous sediments, *Water Resour. Res.*, *23*, 1471–1480.

Zhou, Y., B. Xu, and A. Yu (2001), Numerical investigation of the angle of repose of monosized spheres, *Phys. Rev. E*, *64*, 021301, doi:10.1103/PhysRevE.64.021301.

S. J. de Vet, Faculty of Science, Institute for Biodiversity and Ecosystem Dynamics, University of Amsterdam, PO Box 94248, NL-1090 GE Amsterdam, Netherlands. (s.j.devet@uva.nl)

A. C. in 't Veld and F. N. Postema, Faculty of Aerospace Engineering, Delft University of Technology, Kluyverweg 1, NL-2629 HS Delft, Netherlands. (a.c.intveld@tudelft.nl; f.n.postema@tudelft.nl)

M. G. Kleinhans and H. Markies, Faculty of Geosciences, Utrecht University, PO Box 80115, NL-3508 TC Utrecht, Netherlands. (m.g.kleinhans@uu.nl; h.markies@geo.uu.nl)